BAREKENG: Journal of Mathematics and Its Applications
June 2026 Volume 20 Issue 2 Page 1437–1452
P-ISSN: 1978-7227 E-ISSN: 2615-3017
https://doi.org/10.30598/barekengvol20iss2pp1437-1452

ENHANCING CERVICAL CANCER IMAGES QUALITY: HYBRID SMO-PMD FILTER FOR NOISE REDUCTION

Ach Khozaimi[1], Isnani Darti[2], Syaiful Anam[3*], Wuryansari Muharini Kusumawinahyu[4]

[1,2,3,4] *Department of Mathematics, Faculty of Mathematics and Natural Sciences, Universitas Brawijaya*
Jln. Mayjen Haryono, Lowokwaru, Malang, Jawa Timur, 65145, Indonesia

[1]*Department of Computer Science, Faculty of Engineering, Universitas Trunojoyo Madura*
Jln. Raya Telang, Kabupaten Bangkalan, Madura, Jawa Timur, 69362, Indonesia

*Corresponding author's e-mail: * **syaiful@ub.ac.id***

Article Info

Article History:

Received: 3rd June 2025
Revised: 4th August 2025
Accepted: 24th September 2025
Available online: 26th January 2026

Keywords:

Cervical cancer;
Medical image;
Optimization;
Genetic algorithm;
SMO;
PSO

ABSTRACT

This study presents an image denoising method for cervical cancer images using the Perona–Malik Diffusion (PMD) filter optimized with the Spider Monkey Optimization (SMO) algorithm. The BRISQUE is proposed as the new objective function. The method was simulated on three datasets: SIPaKMeD, Herlev, and Mendeley Liquid-Based Cytology (LBC). Enhanced image quality was evaluated using MSE, SSIM, PSNR, and Entropy. On the SIPaKMeD dataset, the SMO-PMD filter achieved an average MSE of 0.0454, SSIM of 0.9984, PSNR of 62.27 dB, and Entropy of 5.425. The Mendeley dataset recorded an MSE of 0.3991, SSIM of 0.9994, PSNR of 53.08 dB, and Entropy of 5.489. The Herlev dataset achieved an MSE of 8.1191, SSIM of 0.9688, PSNR of 55.77 dB, and Entropy of 5.203. The SMO algorithm was compared with Particle Swarm Optimization (PSO) and Genetic Algorithm (GA). SMO showed better results across all metrics. The proposed method produces images with lower noise, higher structural similarity, and improved visual quality. The stable entropy values across the datasets indicate that essential diagnostic information was preserved. These findings provide a new perspective for enhancing cervical cancer images using a hybrid SMO-PMD filter. A limitation of this study is that experiments were limited to three datasets, and SMO's reliance on extreme κ values might reduce stability in other contexts.

How to cite this article:

A. Khozaimi, I. Darti, S. Anam, and W. M. Kusumawinahyu, "ENHANCING CERVICAL CANCER IMAGES QUALITY: HYBRID SMO-PMD FILTER FOR NOISE REDUCTION," *BAREKENG: J. Math. & App.*, vol. 20, no. 2, pp. 1437-1452, Jun, 2026.

Journal homepage: *https://ojs3.unpatti.ac.id/index.php/barekeng/*
Journal e-mail: *barekeng.math@yahoo.com; barekeng.journal@mail.unpatti.ac.id*

Research Article · Open Access

1. INTRODUCTION

Globally, cervical cancer ranks as the second most prevalent cancer among women [1]. It continues to be a significant public health issue, particularly in developing nations where routine medical examinations are uncommon [2]. Early Pap smear testing is crucial because it can detect abnormal cells before they develop into invasive cancers [3]. Traditionally, Pap smear image analysis is performed manually by cytotechnologists, but this process can be time-consuming and prone to human error [4]. As a result, researchers are developing automated diagnostic systems that rely on digital image processing techniques. Several public datasets are available to support these efforts, including SIPaKMeD, the Mendeley Liquid-Based Cytology (LBC) dataset, and the HErlev Pap Smear Dataset. SIPaKMeD provides five classes of single-cell images that experts have carefully labeled [5]. The Mendeley LBC dataset contains multi-class Pap smear images with diverse visual qualities. Mendeley LBC helps test different analysis methods [6]. The HErlev Pap Smear Dataset is one of the earliest and most widely used collections, which includes images pre-classified into normal and abnormal categories. The Herlev dataset helps researchers benchmark the performance of segmentation, classification, and diagnostic algorithms [7]. These three datasets offer a rich foundation for evaluating and improving automated cervical cancer detection techniques.

Pap smear image quality is crucial for accurate diagnosis and the reliable functioning of automated classification systems [8]. However, Pap smear images frequently encounter issues such as noise and degradation [9]. Staining inconsistencies, microscope lens quality, or problems during digitization cause it. This noise can obscure critical cell components, including the nucleus and cytoplasm, vital for identifying malignant characteristics. Thus, reducing noise from pap smear images is essential to clarify cervical cell images and preserve important details [10]. The study indicates that reducing noise in images enhances their classification accuracy [11]. The PMD filter is a sophisticated image processing tool designed to improve image smoothness while preserving crucial edges [12]. A modified Gaussian function is used to assess the value of each pixel, with the highest values concentrated at the center and gradually diminishing towards the periphery [13]. PMD filters can assist medical professionals in detecting and identifying malignant tumors [14]. In the other study, the PMD filter has been utilized to enhance the performance of deep learning algorithms in classifying cervical cancer [15]. Improving PMD filter performance can be done by tuning its parameters. To overcome the problems with manual tuning, metaheuristic optimization algorithms offer strong and flexible solutions for selecting parameters in complex processing problems [16]. These algorithms simulate how groups act to explore the search space and find the optimal solutions. Particle Swarm Optimization (PSO) is a method that copies the flight patterns of bird flocks [17]. The Genetic Algorithm (GA) is inspired by natural selection and genetics [18]. The Spider Monkey Optimization (SMO) model studies how spider monkeys find food by changing their groups [19]. Each algorithm has its way of exploring and utilizing data to find the best solution for a problem. The SMO algorithm demonstrates superior performance in optimizing UCAV path-planning problems. SMO surpasses other metaheuristic algorithms in the UCAV path-planning problems [20]. This study compared PSO, GA, and SMO to optimize the PMD filter for removing noise from cervical smear images.

The Spider Monkey Optimization (SMO) optimizes the PMD filter with Blind/ Referenceless Image Spatial Quality Evaluator (BRISQUE) as an objective function. BRISQUE is a new objective function for optimizing PMD filter performance to reduce image noise. It examines the appearance of objects based on their spatial arrangement. Using BRISQUE as the objective function allows the optimization process to focus on enhancing images consistent with human perception. BRISQUE is a no-reference image quality assessment. BRISQUE is better than the SSIM and PSNR statistically [21]. This is important for medical imaging applications, where the image quality and how clearly it shows the structure directly impact the accuracy of the diagnosis. The SMO is guided to produce more explicit images by minimizing the BRISQUE score during optimization.

To thoroughly assess the performance of the PMD filter when using each algorithm, this study used five crucial image quality metrics, such as mean squared error (MSE), structural similarity index measurement (SSIM), peak signal-to-noise ratio (PSNR), entropy, and processing time. The MSE and PSNR measure the pixel-level error and signal fidelity, respectively. The SSIM assesses the structural similarity between the original and denoised images, and entropy evaluates the amount of information preserved [22]. This study also examined the time processing for each algorithm, which helped us understand how well the computer performed. The experimental results on the SIPaKMeD, Mendeley LBC, and Herlev datasets show that the hybrid SMO-PMD filter achieved outstanding results across two datasets. The Mendeley dataset's filter achieved an average MSE of 0.3991, SSIM of 0.9994, PSNR of 53.08 dB, and Entropy of 5.489. In the

Herlev dataset, the method achieved an MSE of 8.1191, SSIM of 0.9688, PSNR of 55.77 dB, and Entropy of 5.203. The SMO effectively reduces noise while preserving details. These findings present a new approach for improving cervical cancer images using a hybrid SMO-PMD filter. This study has certain limitations. First, the experiments were conducted on only three datasets, so validation on larger and more diverse clinical collections is still required. Second, while SMO demonstrated broader parameter exploration, its tendency to rely on extreme values of κ may reduce stability when applied beyond the tested settings.

2. RESEARCH METHODS

2.1 Hybrid SMO-PMD Filter

The proposed method and its process are illustrated in Fig. 1. The PMD filter optimization focuses on tuning three parameters: the diffusion coefficient (λ), the edge-stopping threshold (K), and the number of iterations (t). These three parameters balance smoothing noise and preserving important image structures like edges. The SMO algorithm is employed to find the optimal set of parameters. The objective function used in the optimization process is the BRISQUE score, which measures the perceptual quality of images without needing a reference image. Lower scores of BRISQUE indicate better quality. Initially, a population of spider monkeys is created, where each monkey represents a potential solution in the form of a set of PMD parameters. The initial positions are randomly generated within defined bounds. Each solution's fitness is evaluated by applying the PMD filter to the noisy image using the monkey's parameters and calculating the resulting BRISQUE score. The PMD filter and BRISQUE explanations can be found in sections 2.4 and 2.6.

The optimization process then proceeds through several phases. In the Local Leader phase, each monkey updates its position by following the best monkey in its group, encouraging localized improvement. In the Global Leader phase, all monkeys may be influenced by the global best solution found so far. The algorithm also includes Local Leader Decision and Global Leader Decision phases to prevent stagnation by introducing random movements or group splitting if no improvement is detected over a set number of iterations. This process of evaluating, updating, and adapting continues iteratively until the stopping criteria are met. Finally, the best solution found — the spider monkey with the lowest BRISQUE score — provides the optimal combination of λ, K, and t for the PMD filter, this optimized filter achieves high-quality image denoising while preserving critical diagnostic details in cervical cancer images. The SMO algorithm is explained in section 2.5.

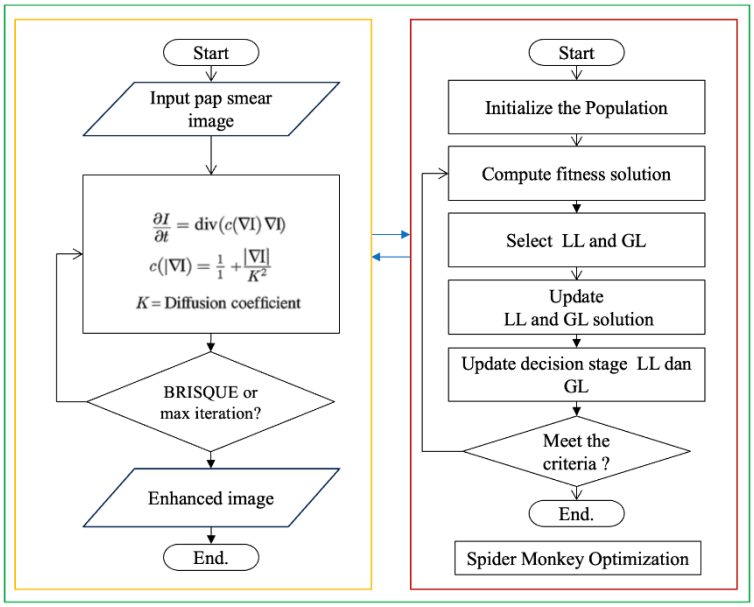

Figure 1. Hybrid SMO-PMD filter

To formalize the hybridization, let the PMD filter be parameterized by three variables: the diffusion coefficient λ, the edge-stopping threshold k, and the number of iterations t. The PMD process can be expressed as:

$$I_{t+1}(x,y) = I_t(x,y) + \lambda \nabla \cdot \left(c(|\nabla I_t(x,y)|)\ \nabla I_t(x,y)\right), \quad (1)$$

where $c(\cdot)$ is the edge-stopping function controlled by k. The optimization goal is to minimize the BRISQUE score $f(\lambda, k, t)$, which evaluates the perceptual quality of the filtered image:

$$min_{\lambda,k,t}\, f\,(\lambda,k,t) = BRISQUE\left(PMD(I;\lambda,k,t)\right), \quad (2)$$

in the SMO algorithm, each spider monkey represents a candidate solution.

$$X_i = (\lambda_i, k_i, t_i),. \quad (3)$$

The update rule in the local leader phase is:

$$X_i^{new} = X_i + r \cdot \left(X_{LL} - X_j\right), \quad (4)$$

where X_{LL} is the best local leader in the group, X_j is a randomly selected solution from the same group, and $r \in [-1,1]$ is a uniform random number. The global best solution X_{GB} is selected based on the lowest BRISQUE score. The hybridization is therefore explicit: the PMD filter provides the denoising mechanism, while SMO adaptively searches for the optimal (λ, k, t) that minimize BRISQUE.

2.2 Pap Smear Image Dataset

The pap smear image quality is crucial for the accurate early diagnosis of cervical cancer. Pap smear images closely examine the structure of cervical cells, particularly the ratio of the nucleus to the cytoplasm, the nucleus's shape, and the cytoplasm's texture. Image quality is essential for two reasons: for cytotechnologists to examine samples manually and for automated diagnostic systems [23]. However, pap smear images are blurry, stained, noisy, and unevenly lit. These issues can obscure critical cellular structures. Low image quality is difficult to diagnose or misinterpret. This implies that image enhancement and denoising are necessary steps in cervical cancer screening pipelines. The noise must be reduced while maintaining essential details, to eliminate noise without losing important information [24].

The SIPaKMeD dataset is a publicly available dataset that researchers use to study the classification of cervical cells. It contains 966 images of cells taken from Pap smear slides using the Papanicolaou method. Each image is labeled into one of five types: superficial, intermediate, parabasal, koilocytotic, metaplastic, or dyskeratotic. The pap smear images were high resolution (2048×1536 pixels) and were taken under controlled conditions using an optical microscope with $400 \times$ magnification [5]. These characteristics make SIPaKMeD a good choice for evaluating cell-level image-analysis tasks. Although the imaging conditions were relatively clean, some images still contained noise with low contrast. This makes it a good test set for image denoising algorithms [25].

The Mendeley LBC dataset has a more diverse and realistic set of images. It closely resembles those encountered in clinical settings. Mendeley LBC contains multiple full-slide pap smear images. Mendeley LBC includes overlapping cells, clumped nuclei, and varying background textures. The samples were stained using different methods, which led to significant differences in the appearance of the images [26]. The image quality also varies across samples. It makes image samples more challenging to improve the image quality. These images have more visual noise and natural imperfections than the SIPaKMeD dataset. Mendeley LBC is ideal for checking the efficacy of denoising techniques. Any improvement algorithm tested on this set of data must make things more straightforward without changing the important cell structures, even when there is a large amount of visual noise [27].

The HErlev Pap Smear dataset is one of the earliest and most widely used cervical cell image analysis collections. It contains 917 single-cell images manually segmented and classified into seven categories, covering both normal and abnormal cell types. The images were captured under $20 \times$ magnification, including detailed cytoplasm and nucleus structures. Cytopathology experts carefully annotated each image, making it a benchmark for classification and segmentation research. The HErlev dataset offers relatively clean images with fewer background artifacts, but still presents challenges related to subtle differences between cell types. It is beneficial for evaluating the accuracy of algorithms in distinguishing normal from precancerous and cancerous cells, as well as for validating image denoising methods that must preserve critical diagnostic features during enhancement [7],[28].

2.3 Software and Hardware Settings

The simulation scenarios were conducted using Python. Python offers powerful image processing and optimization libraries. The PMD filter was implemented in Python. The metaheuristic optimization algorithms (SMO, PSO, and GA) were executed using the MealPy Python library. MealPy is a comprehensive Python-based framework for implementing and comparing a wide range of optimization techniques [29]. We used functions from the OpenCV, scikit-image, and piqa libraries to calculate different image quality metrics. MSE, BRISQUE, SSIM, entropy, and PSNR were used to evaluate the denoised image. All simulations and testing procedures were performed on a computer with Windows 11 as the operating system.

The computer system used in this study had an AMD Ryzen 5 5500 processor with six cores and 12 threads for running multiple tasks simultaneously. The computer system is equipped with 32 GB of DDR4 memory. This memory can handle large image datasets and high-dimensional optimization tasks smoothly. An NVIDIA GeForce RTX 3060 GPU with 12 GB of dedicated VRAM also accelerated specific computational tasks in this computer system. This GPU can involve parallel image processing. This setup provided sufficient computing power to efficiently run all denoising and optimization processes on the SIPaKMeD, Herlev, and Mendeley LBC datasets. This hardware setting ensured we could reproduce the results and minimize the processing time.

2.4 Image Denoising

Image noise reduction is essential in medical image analysis. Pap smear images are cervical images that were used in cervical cancer screening. Pap smear images are noisy with low contrast [30]. Uneven staining, scanning problems, or differences in light use can cause this noise. These problems can make it challenging to see essential cell details, such as the nucleus's location and the cytoplasm's texture. Optimal denoising clarifies pap smear images by reducing noise while retaining the necessary information for a correct diagnosis.

The PMD filter is an algorithm for reducing noise in digital images. This is a special type of image filter that can make the image smoother in some areas while keeping the edges around those areas unchanged [31], [32]. The partial differential equation governing the PMD process is as follows:

$$\frac{\partial I}{\partial t} = \nabla \cdot (c(x,y,t)\nabla I), \tag{5}$$

where I is the image intensity, t is the diffusion time (or iteration), and $\nabla \cdot$ is the divergence operator. The diffusion coefficient $c(x,y,t)$ controls the diffusion rate and is defined in Eq. (6) by Perona and Malik.

$$c(|\nabla I|) = exp\left(-\left(\frac{|\nabla I|}{k} \right)^2 \right), \tag{6}$$

where $|\nabla I|$ is the gradient magnitude, and k is the contrast parameter that determines sensitivity to edges. A lower k value preserves fine details, and a higher value increases smoothing. The PMD filter depends on three primary parameters: the number of times it is run (t), the diffusion coefficient function, and the contrast threshold (k). It is crucial to adjust these settings correctly. This balances noise reduction and edge preservation. This makes PMD highly effective in improving medical images. It does this in situations where the features that help with diagnosis must be maintained [33].

2.5 Meta-heuristics optimization

Meta-heuristic optimization is a group of algorithms designed to find solutions to complex optimization problems that are difficult to solve using traditional methods. These algorithms are inspired by natural processes, such as evolution, swarm intelligence, and social behavior, and are especially effective for problems that are nonlinear, multidimensional, or lack analytical gradients [34]. The main features include random search behavior, exploration of different solutions, adaptability to various problem types, avoidance of local minima through randomness, and innovative search strategies. Meta-heuristics are different from exact optimization methods [35]. They do not guarantee a global optimum but can efficiently find good-quality solutions in a reasonable amount of time. It has three main advantages. First, they are simple to use. Second, they can be used in various ways. Third, they are strong even when the data are incomplete or incorrect. In image-processing applications such as image denoising, meta-heuristic algorithms help adjust filter parameters when the objective function (e.g., visual quality or non-differentiable metrics such as

BRISQUE) is challenging to analyze. This makes meta-heuristic approaches, such as particle swarm optimization (PSO), genetic algorithm (GA), and spider monkey optimization (SMO), very effective for improving complex image enhancement techniques.

The SMO algorithm is a worldwide optimization technique that draws inspiration from the foraging behavior of spider monkeys. It mimics how these animals follow leaders, share information, and divide into smaller groups to explore their environment [36], [37]. In SMO, each spider monkey represents a possible solution to a problem and is placed in a D-dimensional space using the formula:

$$SM_{k,j} = SM_{min,j} + R \times \left(SM_{max,j} - SM_{min,j}\right), \tag{7}$$

where R is a random number between 0 and 1, and $SM_{min,j}$ and $SM_{max,j}$ the lower and upper bounds of the search space for each dimension.

The optimization process involves several phases. In the Local Leader (LL) phase, each monkey updates its position based on the best monkey (local leader) in its group using the equation:

$$SM_{new\,i,j} = SM_{i,j} + R \times \left(Leader_{k,j} - SM_{i,j}\right) + U(-1,1) \times \left(SM_{r,j} - SM_{i,j}\right), \tag{8}$$

where $SM_{r,j}$ is a randomly chosen monkey from the same group, and $U(-1,1)$ it is a uniform random number between -1 and 1. If this new position improves the result, it is accepted.

In the Global Leader (GL) phase, monkeys may follow the global best solution with a probability calculated as:

$$prob_i = 0.9 \times \frac{fitness_i}{\underset{fitness}{max}} + 0.1. \tag{9}$$

This gives monkeys with better solutions higher chances to explore new positions.

SMO includes the Local Leader Decision (LLD) and Global Leader Decision (GLD) phases to maintain diversity and prevent stagnation. If there is no improvement after several iterations, monkeys may randomly change positions or split into subgroups to explore better areas. These collaborative and adaptive strategies make SMO effective for solving complex optimization problems, such as tuning parameters in image denoising tasks.

2.6 Image Quality Assessment

This study used five main metrics to evaluate the image quality: MSE, SSIM, PSNR, entropy, and BRISQUE. These metrics show how well the processed images maintain the original images' quality, structure, details, and visual quality [38], [39]. Each metric shows a different aspect of image quality and provides a thorough and objective evaluation.

1. Mean Squared Error (MSE):

   MSE quantifies the mean of the squared differences between the original and the processed (filtered) images. A smaller MSE value suggests that the filtered image more closely resembles the original. The MSE is determined using this formula:

$$\text{MSE} = \frac{1}{mn}\sum_{i=1}^{m}\sum_{j=1}^{n}[\text{I}(i,j) - K(i,j)]^2\,, \tag{10}$$

   where I is the original image, K is the filtered image, and $m \times n$ is the image size.

2. Structural Similarity Index (SSIM):

   SSIM evaluates how alike two images are by examining their brightness, contrast, and structure. The resulting values span from -1 to 1, 1 signifying complete similarity. The SSIM formula is as follows:

$$\text{SSIM}(x,y) = \frac{\left(2\mu_x\mu_y + C_1\right)\left(2\sigma_{xy} + C_2\right)}{\left(\mu_x^2 + \mu_y^2 + C_1\right)\left(\sigma_x^2 + \sigma_y^2 + C_2\right)}, \tag{11}$$

   where μ is the mean, σ^2 is the variance, and σ_{xy} is the covariance of the images.

3. Peak Signal-to-Noise Ratio (PSNR):

The PSNR measures the quality of the filtered image based on the MSE. A higher PSNR value indicates a better quality. This formula calculates PSNR.

$$\text{PSNR} = 10 \cdot \log_{10}\left(\frac{MAX_I^2}{MSE}\right), \tag{12}$$

where MAX_I is the maximum possible pixel value (255 for 8-bit images).

4. Entropy:

Entropy measures the amount of information or details in an image. Higher entropy indicates that the image contains more texture or variation. This formula calculates entropy.

$$\text{Entropy} = -\sum_i p(i)\log_2 p\,(i), \tag{13}$$

where $p(i)$ is the probability of pixel intensity i.

5. Blind/Referenceless Image Spatial Quality Evaluator (BRISQUE)

BRISQUE is a method for measuring the quality of a digital image. The original image is not required to use BRISQUE. BRISQUE belongs to the NR-IQA metrics, so it is flexible and can be used with different types of images. BRISQUE uses natural scene statistics (NSS) to calculate these statistics. NSS is a method for measuring the statistics of natural images (images that have not been altered). The BRISQUE algorithm uses NSS to understand the pixel intensity distribution of an image. BRISQUE uses the distribution of mean-subtracted contrast-normalized (MSCN) coefficients to extract features from an image [40]. The MSCN coefficients are calculated using the following equation:

a. MSCN coefficients:

$$I(i,j) = \frac{I(i,j) - \mu(i,j)}{\sigma(i,j) + C}, \tag{14}$$

with $I(i,j)$ is the intensity of the image, C a small constant to avoid division by zero,

$$\mu(i,j) = \sum_{k=-K}^{K}\sum_{l=-K}^{L} w(k,l)I(i+k,j+l)\,, \tag{15}$$

$$\sigma(i,j) = \sqrt{\sum_{k=-K}^{K}\sum_{l=-K}^{L} w(k,l)\big(I(i+k,j+l) - \mu(i,j)\big)^2}\,, \tag{16}$$

$w(\mathrm{k},\mathrm{l})$ is the Gaussian kernel.

b. Feature Extraction

BRISQUE extracts features from the histogram of the MSCN coefficients and the pair products derived from them: horizontal (H), vertical (V), main diagonal (D1), and secondary diagonal (D2), as shown in Fig. 2.

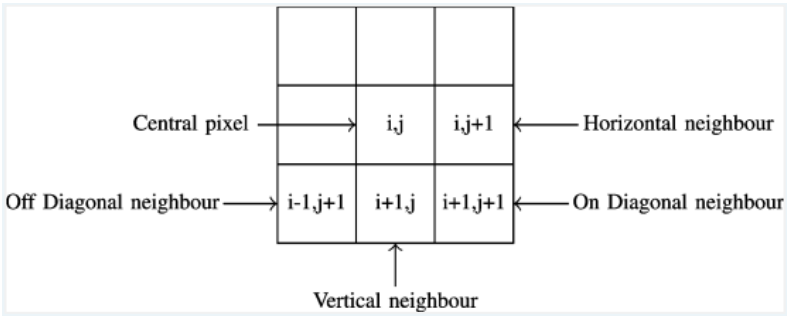

Figure 2. Coefficients MSCN

c. Generalized Gaussian Distribution (GGD)

The extracted features are fed to the GGD to calculate the distribution parameters.

$$f(x;\alpha,\sigma) = \frac{\alpha}{2\beta\Gamma(1/\alpha)} exp\left(-\left(\frac{|x|}{\beta}\right)^{\alpha}\right), \quad (17)$$

with Γ is the gamma function and $\beta = \sigma\sqrt{\frac{\Gamma(1/\alpha)}{\Gamma(3/\alpha)}}$.

3. RESULTS AND DISCUSSION

Table 1 compares the original and enhanced images from the SIPaKMeD, Mendeley LBC, and Herlev datasets. Significant improvements in image quality can be observed when comparing the original images with those processed using the optimization-based PMD filter methods. These enhancements are evident in the reduction of noise, sharper cell contours, and improved image clarity. Meanwhile, the visual differences among the images enhanced using the three hybrid methods, the Hybrid PSO-PMD Filter, the Hybrid GA-PMD Filter, and the Hybrid SMO-PMD Filter, appear minimal. All three methods produce images of similarly high visual quality. It is difficult to determine the superior approach based solely on visual inspection. However, objective evaluation using the BRISQUE metric offers a more precise image quality assessment. BRISQUE measures distortions based on the natural statistical characteristics of images. Lower BRISQUE scores indicate better image quality. The test results demonstrate that the Hybrid SMO-PMD Filter consistently achieves the lowest BRISQUE scores compared to other methods. The Hybrid SMO-PMD Filter is statistically considered to have optimal image quality.

In addition to visual assessment, the enhanced images' quality was evaluated using several quantitative metrics, including MSE, SSIM, PSNR, Entropy, BRISQUE, and computational time. The simulations were conducted on 10 images from each dataset (SIPaKMeD, Mendeley LBC, and Herlev datasets). The simulation results for each evaluation metric were averaged to ensure reliable and representative measurements. The detailed simulation results for the three datasets used in this study are presented and discussed in Sections 3.1 to 3.4.

Table 1. The BRISQUE Score of Original Images vs Enhanced Images

Image Datasets	Original Image	PSO-PMD Filter	GA-PMD Filter	SMO-PMD Filter
SIPaKMeD (Brisque score)	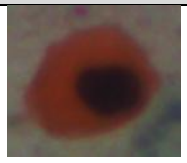	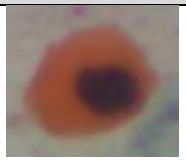	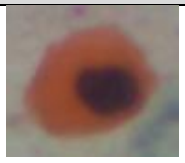	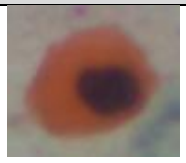
	67.75482	58.63072	58.93625	**57.95712**
Mendeley LBC (Brisque score)	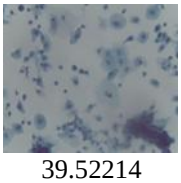	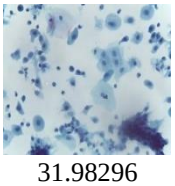	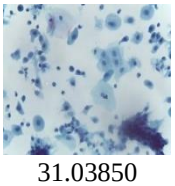	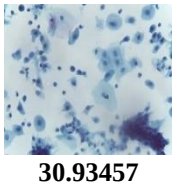
	39.52214	31.98296	31.03850	**30.93457**
Herlev (Brisque score)	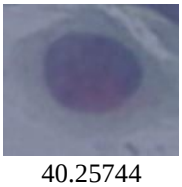	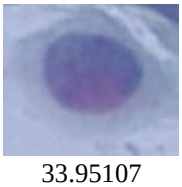	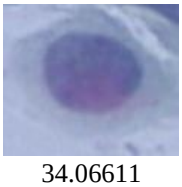	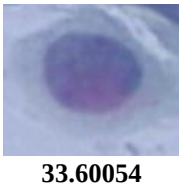
	40.25744	33.95107	34.06611	**33.60054**

3.1 Exploration Analysis of Optimizers

To quantify the exploration ability of each optimizer, we examined the distribution of PMD parameters discovered in the Mendeley dataset. Fig. 3 presents boxplots of the two parameters. In terms of κ in Fig. 3 (a), SMO often reached the extremes of the search space (around 10 or 100), while PSO and GA were more focused on intermediate ranges. For λ in Fig. 3 (b), SMO solutions were mainly centred around 0.01, whereas

PSO and GA showed wider variation. The number of iterations was generally consistent across methods (mostly 5–7), but SMO demonstrated reliable convergence with less minor variance across methods (mostly 5–7), but SMO showed consistent convergence with less minor variance.

Parameter coverage is further illustrated in Fig. 4 (a), which plots κ against λ. SMO explored the extreme corners of the search space (very low or very high κ values combined with near-constant λ), whereas GA and PSO clustered in more limited intermediate regions. This suggests that SMO employed a more aggressive exploration strategy, contrasting with the more exploitative behavior of GA and PSO. We also compared convergence behavior by plotting BRISQUE values against the number of iterations Fig. 4 (b). SMO showed steady improvements across iterations, maintaining progress until convergence. By contrast, PSO and GA often plateaued earlier, indicating premature convergence.

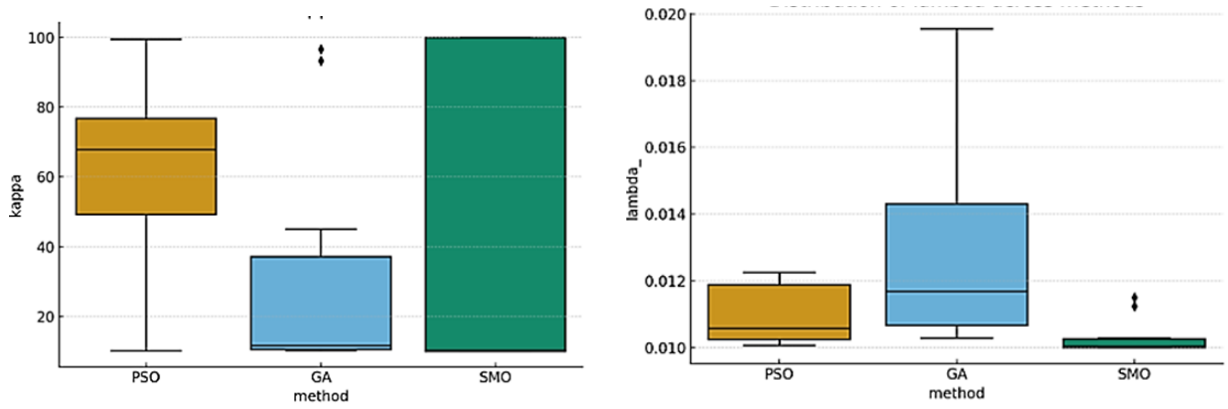

(a) **(b)**

Figure 3. Distribution (a) κ Across Methods and (b) λ Across Methods

Population diversity was approximated using the variance of the discovered parameters across independent runs. SMO exhibited higher variance in κ, reflecting broader coverage of the search space, but lower variance in λ, suggesting stable convergence toward a perceptually optimal region. In contrast, GA and PSO maintained narrower ranges, which limited their ability to escape local minima. Statistical testing confirmed these trends: the distributions of λ differed significantly among methods (Kruskal–Wallis, $p = 0.003$), while the differences in κ were not statistically significant ($p = 0.457$). These simulation results substantiate the claim that SMO demonstrates stronger exploration capability, not by random scattering, but by systematically pushing parameter searches toward extreme and informative regions of the domain. This exploratory behavior directly translates into more effective noise reduction and superior denoising performance compared to GA and PSO.

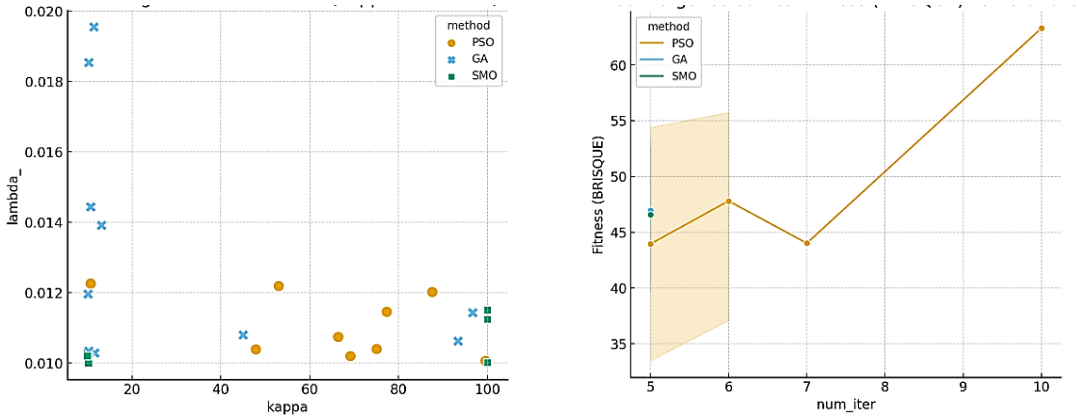

(a) (b)

Figure 4. (a) Coverage Search Domain κ, λ and (b) Convergence Fitness Function vs Iteration

3.2 SIPaKMeD Dataset

Table 2 presents the optimization results of the PMD filter on the SIPaKMeD dataset. SMO produced the most promising outcomes across nearly all evaluation metrics among the tested algorithms. It achieved the lowest average MSE of 0.0454, indicating minimal deviation from the original images at the pixel level. The SSIM score of 0.9984 further confirmed that SMO preserved the structural integrity of cervical cell features, which is critical for accurate classification and analysis. Its PSNR value of 62.27 dB was the highest among the methods, demonstrating strong noise suppression and fidelity preservation. From a perceptual standpoint, the SMO also yielded the lowest BRISQUE score of 36.24, suggesting improved visual quality without requiring a ground truth reference. These results collectively highlight SMO's effectiveness in enhancing microscopic cell images by producing visually clear and diagnostically valuable outputs.

In comparison, PSO achieved moderate results, with an MSE of 0.0617, SSIM of 0.9980, and PSNR of 60.72 dB. While these values indicate reasonably good image quality, PSO's slightly higher BRISQUE score (36.77) suggests marginally less perceptual quality than SMO. The GA algorithm demonstrated the lowest performance among the three, with the highest MSE (0.0670) and lowest PSNR (60.53 dB), though it did retain a strong SSIM score of 0.9979. Interestingly, the entropy values were virtually identical across all three methods (around 5.42), suggesting that all approaches maintained similar texture and information content within the images. However, the trade-off becomes evident in processing time: SMO took an average of 148.26 seconds, significantly longer than PSO (90.13 seconds) and GA (83.19 seconds).

Despite its longer runtime, SMO's superior performance across objective (MSE, PSNR) and perceptual (SSIM, BRISQUE) metrics makes it an ideal candidate for applications requiring high image fidelity, such as automated cervical cancer screening systems. In clinical practice, the cost of slower processing is often outweighed by the importance of diagnostic accuracy. SMO's hierarchical search strategy and dynamic grouping allow it to explore the solution space more thoroughly, avoiding local optima that commonly hinder GA and PSO. These characteristics make it particularly suitable for complex, nonlinear optimization tasks like PMD filtering, where multiple competing objectives must be balanced simultaneously.

Table 2. PMD filter optimization on SIPaKMeD dataset

Algorithm	MSE	SSIM	PSNR	Entropy	BRISQUE	Time
PSO	0.0617	0.9980	60.7169	5.4250	36.7708	90.1324
GA	0.0670	0.9979	60.5267	5.4249	37.0787	**83.1949**
SMO	**0.0454**	**0.9984**	**62.2706**	**5.4251**	**36.2366**	148.2581

3.3 Mendeley LBC dataset

On the Mendeley LBC dataset, SMO again delivered the best overall performance, as shown in Table 3. It achieved the lowest MSE (0.3991), indicating higher pixel-wise accuracy in noise removal, and the highest PSNR (53.08 dB), signifying a higher quality reconstruction. The SSIM score of 0.9994 was nearly perfect, suggesting that structural patterns, particularly nuclear and cytoplasmic boundaries, were well-preserved, essential for detecting morphological abnormalities in Pap smear images. Moreover, SMO recorded the lowest BRISQUE score (46.60), emphasizing its strength in producing visually coherent and natural-looking images from a human perception standpoint. Notably, it also exhibited the highest entropy value (5.4888), indicating richer textural detail and a higher degree of image information post-processing.

Compared to the other optimization techniques, GA achieved slightly higher entropy (5.4878) than PSO but lower than SMO, and demonstrated a relatively low MSE (0.5339) with a PSNR of 51.29 dB. Although it performed faster (44.49 seconds) than PSO and SMO, its higher BRISQUE score (46.98) indicates slightly inferior visual quality. PSO, in contrast, had the highest MSE (0.7325) and the lowest PSNR (49.98 dB), along with the worst BRISQUE score (47.43), despite achieving a high SSIM of 0.9988. These results suggest that while PSO maintains a strong structural resemblance, it fails to reduce noise and artifacts as effectively as SMO or GA. Regarding processing time, PSO completed optimization in 50.28 seconds—faster than SMO but slower than GA.

The results reaffirm SMO's strength in quantitative and perceptual metrics, positioning it as the most suitable algorithm for PMD filter optimization on the Mendeley dataset. This capability is particularly relevant in cytopathological diagnostics, where image quality is critical in accurate interpretation by automated systems and medical experts. While SMO's processing time was slightly higher, the quality gains

are substantial and justifiable in contexts such as early cervical cancer detection, where high accuracy can significantly affect patient outcomes.

Table 3. PMD filter optimization on the Mendeley LBC dataset

Algorithm	MSE	SSIM	PSNR	Entropy	BRISQUE	Time
PSO	0.7325	0.9988	49.9801	5.4867	47.4270	50.2844
GA	0.5339	0.9989	51.2969	5.4878	46.9766	**44.4851**
SMO	**0.3991**	**0.9994**	**53.0825**	**5.4888**	**46.5955**	81.8744

To evaluate the relationship between execution time and the quality improvements achieved by SMO–PMD, we analyzed all per-image optimization results on the Mendeley LBC dataset ($n = 10$). Fig. 5 (a) shows a scatter plot of runtime versus PSNR for each run; Fig. 5 (b) presents runtime versus BRISQUE; and Fig. 5 (c) depicts the Pareto frontier for PSNR versus runtime. On average, SMO achieved a 6.20% increase in PSNR compared to PSO (95% CI ±2.05%) and 3.50% compared to GA (95% CI ±2.83%). BRISQUE scores also improved, with a mean reduction of −1.98% relative to PSO (95% CI ±0.83%) and −0.78% relative to GA (95% CI ±0.42%). However, these improvements came with longer runtimes: SMO required +62.85% more time than PSO (95% CI ±2.69%) and +84.08% more than GA (95% CI ±2.69%). At the per-image level, PSNR(SMO) exceeded PSO in all 10 cases and GA in 9/10 cases; BRISQUE(SMO) was better than both in all 10 cases. The Pareto frontier analysis showed that several GA runs remained non-dominated, offering lower runtime with comparable quality. In contrast, SMO appeared on the frontier only once, achieving the highest PSNR but at a significantly higher computational cost. These findings confirm that SMO–PMD consistently improves image quality, but the corresponding runtime trade-off must be carefully considered for practical use.

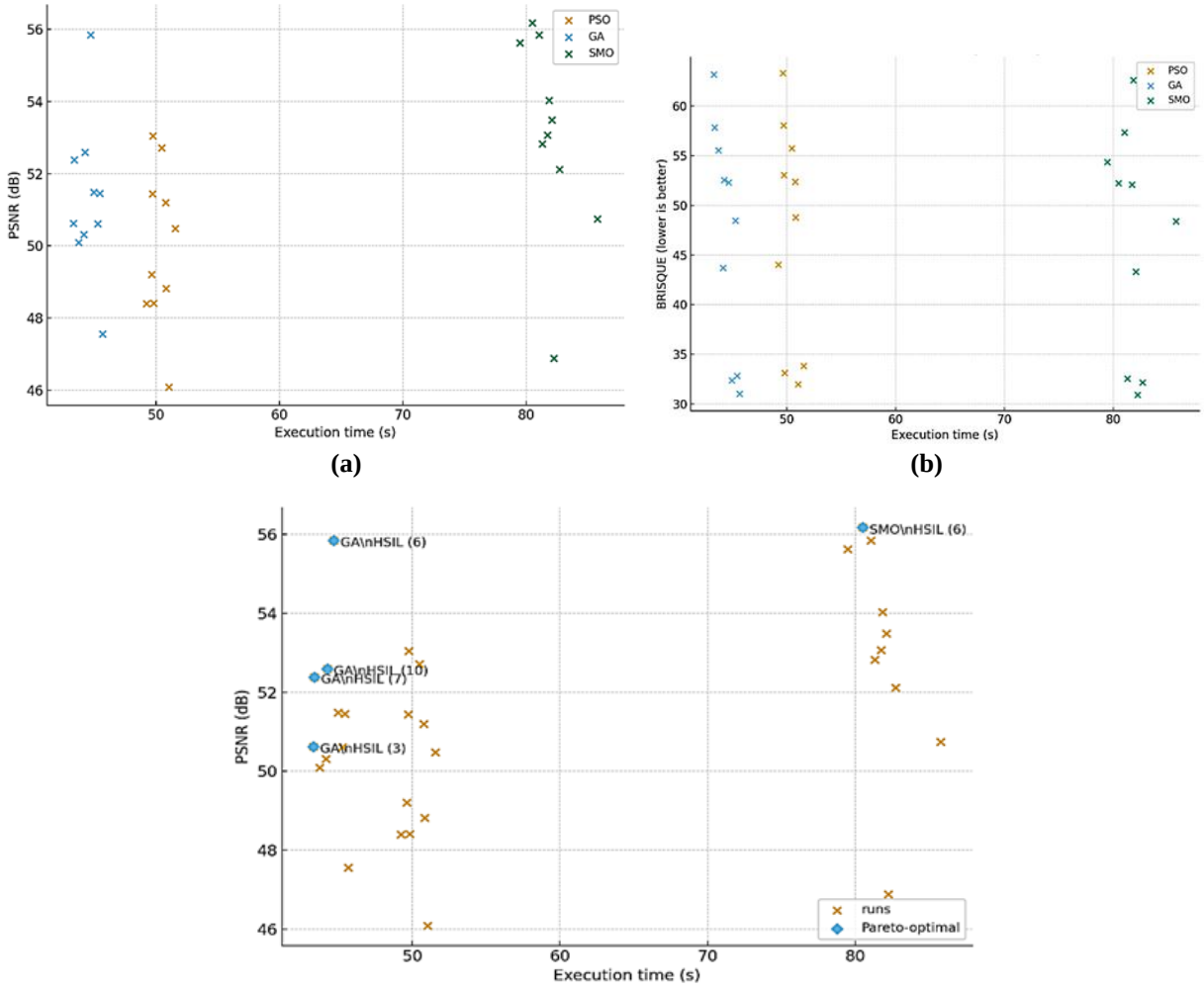

Figure 5. Time–Quality Trade-Off on Mendeley LBC Dataset. (a) Runtime vs PSNR, (b) Runtime vs BRISQUE, (c) Pareto Frontier for Runtime vs PSNR

3.4 Herlev Pap Smear Dataset

The Herlev Pap Smear dataset further validated the SMO algorithm's superiority in PMD filter optimization, which was shown in Table 4. SMO achieved the highest SSIM (0.9688) and PSNR (55.77 dB), indicating robust noise reduction and structure preservation, even though its MSE (8.1191) was slightly higher than PSO's (7.9281). The entropy (5.2031) and lowest BRISQUE score (36.36) confirmed the algorithm's ability to preserve intricate cell features and produce perceptually superior images. Given that BRISQUE was used as the objective function during optimization, the results reflect successful convergence to perceptually optimal solutions.

While PSO achieved the lowest MSE, its slightly lower SSIM (0.9687) and higher BRISQUE (36.79) suggest a trade-off between noise suppression and structure preservation. GA, on the other hand, yielded the weakest results, with the highest MSE (8.14), lowest SSIM (0.9673), and highest BRISQUE score (37.06), though it had the fastest processing time (28.18 seconds). SMO's processing time (50.43 seconds) was significantly higher but acceptable in clinical contexts where diagnostic accuracy is prioritized. The near-identical entropy values across all three methods (≈5.203) indicate that none of the algorithms excessively simplified or distorted the image content during denoising.

In conclusion, the hybrid SMO-PMD approach is the most effective technique across all tested datasets. Its ability to produce high-quality denoised images with preserved structural and perceptual features makes it an ideal candidate for enhancing Pap smear images in automated screening systems. The slightly increased computational time is a reasonable trade-off for improving diagnostic relevance, robustness, and visual quality. These findings strongly support the integration of SMO into medical image processing pipelines, particularly in systems aimed at cervical cancer detection and cytological analysis.

Table 4. PMD Filter Optimization on the HerLev Dataset

Algorithm	MSE	SSIM	PSNR	Entropy	BRISQUE	Time
PSO	**7.9281**	0.9687	54.8602	5.2030	36.7978	30.4619
GA	8.1424	0.9673	53.4722	5.2023	37.0565	**28.1789**
SMO	8.1191	**0.9688**	**55.7737**	**5.2031**	**36.3616**	50.4331

To assess the relationship between execution time and quality improvement provided by SMO–PMD, we analyzed per-image optimization results on the Herlev dataset ($n = 10$). Fig. 6 (a) shows runtime versus PSNR for each run, Fig. 6 (b) shows runtime versus BRISQUE, and Fig. 6 (c) depicts the Pareto frontier for PSNR versus runtime. On average, SMO produced a 1.57% increase in PSNR compared to PSO (95% CI ±1.48%) and a 4.15% increase compared to GA (95% CI ±2.50%). BRISQUE scores also improved, with mean reductions of 1.30% versus PSO (95% CI ±0.64%) and 2.18% versus GA (95% CI ±1.94%). These improvements were achieved at the cost of longer runtimes: SMO required +67.61% more time than PSO (95% CI ±6.98%) and +79.48% more than GA (95% CI ±2.84%). At the per-image level, PSNR(SMO) exceeded PSO for 7/10 images and GA for 8/10 images; BRISQUE(SMO) was better than both comparators on all 10 images. Pareto analysis shows several GA and PSO runs remain non-dominated (favorable runtime with competitive PSNR). At the same time, SMO occupies Pareto positions when it attains the highest PSNR at substantially higher computational cost. Taken together, the Herlev results indicate that SMO–PMD can improve image quality but imposes a substantial runtime penalty; whether this trade-off is acceptable depends on application constraints.

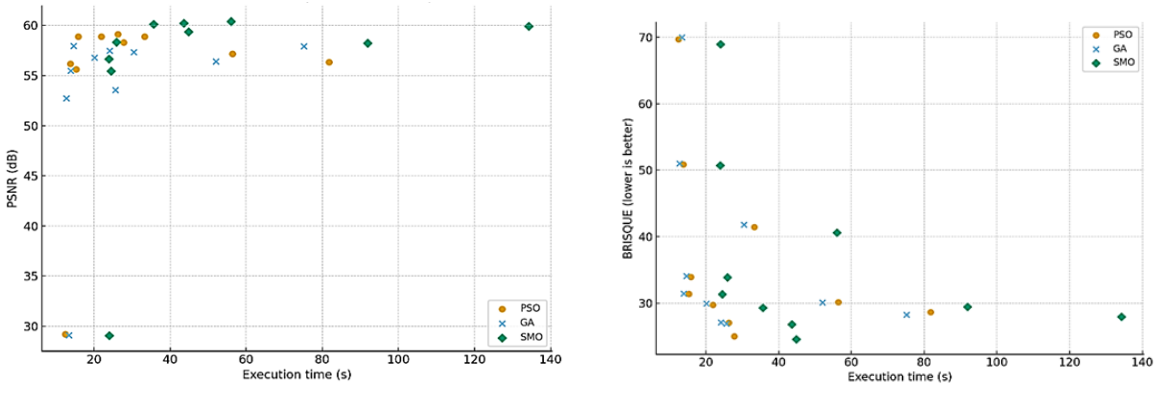

(a) **(b)**

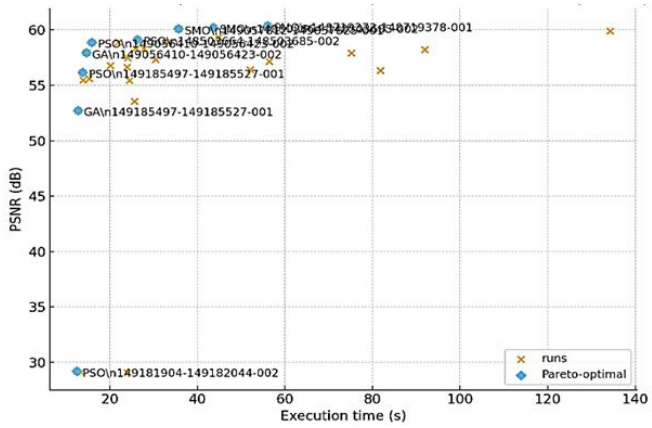

(c)

Figure 6. Time–quality trade-off on Herlev datasets. (a) runtime vs PSNR, (b) runtime vs BRISQUE, (c) Pareto frontier for runtime vs PSNR

4. CONCLUSIONS

This study introduced a hybrid SMO–PMD filter to enhance the quality of cervical images. The PMD filter effectively reduced image noise, while the Spider Monkey Optimization (SMO) algorithm was employed to optimize the filter parameters. By using the BRISQUE score as an objective function, the optimization was directed toward perceptually relevant solutions. Across three benchmark datasets (SIPaKMeD, Mendeley LBC, and Herlev), SMO–PMD demonstrated competitive—and in several cases superior—performance compared to GA–PMD and PSO–PMD. On the Mendeley dataset, SMO achieved a mean PSNR of 53.08 ± 1.72 dB, compared with 49.98 ± 1.35 dB for PSO and 51.30 ± 1.32 dB for GA. This corresponds to an improvement of ~6.2% over PSO and ~3.5% over GA. BRISQUE scores showed smaller differences, with averages of 46.60 ± 7.03 (SMO), 46.98 ± 7.13 (GA), and 47.43 ± 6.95 (PSO). These quality gains came at the cost of increased runtime: SMO required ~60–70% longer than GA and PSO on average. This time, the quality trade-off is important to consider for practical deployment. Representative per-image statistics indicated consistent improvements across runs, and paired significance testing (Kruskal-Wallis, p<0.05) confirmed significant differences in parameter distributions, particularly for λ. Nonetheless, several limitations should be acknowledged. First, experiments were limited to three datasets; further validation on larger and more diverse clinical datasets is necessary. Second, although SMO showed broader parameter exploration, its reliance on extreme values of κ suggests potential instability if applied outside the tested settings. The hybrid SMO–PMD filter can be considered a competitive and, in many cases, superior approach for enhancing Pap smear images. Future work should extend this analysis by incorporating alternative objective functions, additional no-reference quality measures, and integration with deep learning-based diagnostic systems.

Author Contributions

Ach Khozaimi: Conceptualization, Data Curation, Formal Analysis, Funding Acquisition, Methodology, Resources, Software, Visualization, Writing - Original Draft. Isnani Darti: Conceptualization, Data Curation, Investigation, Methodology, Project Administration, Supervision, Validation, Writing - Review and Editing. Syaiful Anam: Conceptualization, Data Curation, Funding Acquisition, Investigation, Methodology, Resources, Software, Supervision, Validation, Visualization, Writing - Review and Editing. Wuryansari Muharini Kusumawinahyu: Formal Analysis, Investigation, Project Administration, Supervision, Validation, Writing - Review and Editing. All authors have read and approved the final version of the manuscript.

Funding Statement

This research was supported by the Ministry of Higher Education, Science, and Technology of the Republic of Indonesia, in collaboration with the Indonesian Education Foundation (LPDP). Financial assistance was provided through the Centre for Higher Education Funding and Assessment (PPAPT) as part of the Indonesian Education Scholarship (BPI) program.

Acknowledgment

The authors wish to convey their profound gratitude to the High-Performance Computing (HPC) Team at the Faculty of Mathematics and Natural Sciences, Universitas Brawijaya, Indonesia, for their unwavering support. Their provision of critical computing resources and infrastructure significantly contributed to the successful completion of this work study.

Declarations

The authors declare no competing interests.

Declaration of Generative AI and AI-assisted Technologies

Generative AI tools (e.g., ChatGPT) were used solely for language refinement, including grammar, spelling, and clarity. The scientific content, analysis, interpretation, and conclusions were developed entirely by the authors. All final text was reviewed and approved by the authors.

REFERENCES

[1] G. Curigliano, "MANAGEMENT OF CARDIAC DISEASE IN CANCER PATIENTS THROUGHOUT ONCOLOGICAL TREATMENT: ESMO CONSENSUS RECOMMENDATIONS," *Annals of Oncology*, vol. 31, no. 2, pp. 171–190, 2020.

[2] D. A. Jia, B. Zhengyi Li, and C. Chuanwang Zhang, "DETECTION OF CERVICAL CANCER CELLS BASED ON STRONG FEATURE CNN-SVM NETWORK," *Neurocomputing*, vol. 411, pp. 112–127, Oct. 2020. doi: https://doi.org/10.1016/j.neucom.2020.06.006

[3] L. Allahqoli *et al.*, "DIAGNOSIS OF CERVICAL CANCER AND PRE-CANCEROUS LESIONS BY ARTIFICIAL INTELLIGENCE: A SYSTEMATIC REVIEW," *Diagnostics*, vol. 12, no. 11, pp. 1–32, 2022. doi: https://doi.org/10.3390/diagnostics12112771

[4] Y.-M. Lee, B. Lee, N.-H. Cho, and J. H. Park, "BEYOND THE MICROSCOPE: A TECHNOLOGICAL OVERTURE FOR CERVICAL CANCER DETECTION," *Diagnostics*, vol. 13, no. 19, p. 3079, Sep. 2023. doi: https://doi.org/10.3390/diagnostics13193079

[5] M. E. Plissiti, P. Dimitrakopoulos, G. Sfikas, C. Nikou, O. Krikoni, and A. Charchanti, "SIPAKMED: A NEW DATASET FOR FEATURE AND IMAGE BASED CLASSIFICATION OF NORMAL AND PATHOLOGICAL CERVICAL CELLS IN PAP SMEAR IMAGES," in *2018 25th IEEE International Conference on Image Processing (ICIP)*, 2018, pp. 3144–3148. doi: https://doi.org/10.1109/icip.2018.8451588

[6] O. Yaman and T. Tuncer, "EXEMPLAR PYRAMID DEEP FEATURE EXTRACTION BASED CERVICAL CANCER IMAGE CLASSIFICATION MODEL USING PAP-SMEAR IMAGES," *Biomed Signal Process Control*, vol. 73, p. 103428, Mar. 2022. doi: https://doi.org/10.1016/j.bspc.2021.103428

[7] B. Z. Wubineh, A. Rusiecki, and K. Halawa, "SEGMENTATION AND CLASSIFICATION TECHNIQUES FOR PAP SMEAR IMAGES IN DETECTING CERVICAL CANCER: A SYSTEMATIC REVIEW," *IEEE Access*, vol. 12, pp. 118195–118213, 2024. doi: https://doi.org/10.1109/access.2024.3447887

[8] A. Khozaimi and W. Firdaus Mahmudy, "NEW INSIGHT IN CERVICAL CANCER DIAGNOSIS USING CONVOLUTION NEURAL NETWORK ARCHITECTURE," *IAES International Journal of Artificial Intelligence (IJ-AI)*, vol. 13, no. 3, p. 3092, Sep. 2024. doi: https://doi.org/10.11591/ijai.v13.i3.pp3092-3100

[9] K. P. Win, Y. Kitjaidure, K. Hamamoto, and T. Myo Aung, "COMPUTER-ASSISTED SCREENING FOR CERVICAL CANCER USING DIGITAL IMAGE PROCESSING OF PAP SMEAR IMAGES," *Applied Sciences*, vol. 10, no. 5, p. 1800, Mar. 2020. doi: https://doi.org/10.3390/app10051800

[10] W. He, T. Liu, Y. Han, W. Ming, J. Du, Y. Liu, Y. Yang, L. Wang, Z. Jiang, Y. Wang, J. Yuan, and C. Cao, "A REVIEW: THE DETECTION OF CANCER CELLS IN HISTOPATHOLOGY BASED ON MACHINE VISION," *Comput Biol Med*, vol. 146, p. 105636, Jul. 2022.

[11] M. Zhao *et al.*, "SEENS: NUCLEI SEGMENTATION IN PAP SMEAR IMAGES WITH SELECTIVE EDGE ENHANCEMENT," *Future Generation Computer Systems*, vol. 114, pp. 185–194, Jan. 2021. doi: https://doi.org/10.1016/j.future.2020.07.045

[12] V. Kamalaveni, R. A. Rajalakshmi, and K. A. Narayanankutty, "IMAGE DENOISING USING VARIATIONS OF PERONA-MALIK MODEL WITH DIFFERENT EDGE STOPPING FUNCTIONS," *Procedia Comput Sci*, vol. 58, pp. 673–682, 2015. doi: https://doi.org/10.1016/j.procs.2015.08.087

[13] S. Anam, Z. Fitriah, and N. Shofianah, "HYBRID OF THE PMD FILTER, THE K-MEANS CLUSTERING METHOD AND THE LEVEL SET METHOD FOR EXUDATES SEGMENTATION," in *Proceedings of the International Conference on Mathematics and Islam*, SCITEPRESS - Science and Technology Publications, Jan. 2018, pp. 108–116, 2018. doi: https://doi.org/10.5220/0008517901080116

[14] V. E. S., "BILATERAL PERONA-MALIK DIFFUSION FILTERING BASED TOPOLOGICAL MULTITUDE FEATURE VECTOR FOR BREAST CANCER DETECTION," *Journal of Research on the Lepidoptera*, vol. 51, no. 1, pp. 110–128, Feb. 2020. doi: https://doi.org/10.36872/lepi/v51i1/301010

[15] M. M. Rahaman, "A SURVEY FOR CERVICAL CYTOPATHOLOGY IMAGE ANALYSIS USING DEEP LEARNING," *IEEE Access*, vol. 8, pp. 61687–61710, 2020.

[16] M. A. Elaziz *et al.*, "ADVANCED METAHEURISTIC OPTIMIZATION TECHNIQUES IN APPLICATIONS OF DEEP NEURAL NETWORKS: A REVIEW," *Neural Comput Appl*, vol. 33, no. 21, pp. 14079–14099, Nov. 2021. doi: https://doi.org/10.1007/s00521-021-05960-5
[17] K. Aurangzeb, S. Aslam, M. Alhussein, R. A. Naqvi, M. Arsalan, and S. I. Haider, "CONTRAST ENHANCEMENT OF FUNDUS IMAGES BY EMPLOYING MODIFIED PSO FOR IMPROVING THE PERFORMANCE OF DEEP LEARNING MODELS," *IEEE Access*, vol. 9, pp. 47930–47945, 2021. doi: https://doi.org/10.1109/access.2021.3068477
[18] F. Johnson, A. Valderrama, C. Valle, B. Crawford, R. Soto, and R. Nanculef, "AUTOMATING CONFIGURATION OF CONVOLUTIONAL NEURAL NETWORK HYPERPARAMETERS USING GENETIC ALGORITHM," *IEEE Access*, vol. 8, pp. 156139–156152, 2020. doi: https://doi.org/10.1109/access.2020.3019245
[19] D. Kumari, A. Sinha, S. Dutta, and P. Pranav, "OPTIMIZING NEURAL NETWORKS USING SPIDER MONKEY OPTIMIZATION ALGORITHM FOR INTRUSION DETECTION SYSTEM," *Sci Rep*, vol. 14, no. 1, p. 17196, Jul. 2024. https://doi.org/10.1038/s41598-024-68342-6
[20] H. Zhu, Y. Wang, Z. Ma, and X. Li, "A COMPARATIVE STUDY OF SWARM INTELLIGENCE ALGORITHMS FOR UCAV PATH-PLANNING PROBLEMS," *Mathematics*, vol. 9, no. 2, pp. 1–31, Jan. 2021. doi: https://doi.org/10.3390/math9020171
[21] A. Mittal, A. K. Moorthy, and A. C. Bovik, "NO-REFERENCE IMAGE QUALITY ASSESSMENT IN THE SPATIAL DOMAIN," *IEEE Transactions on Image Processing*, vol. 21, no. 12, pp. 4695–4708, Dec. 2012. doi: https://doi.org/10.1109/tip.2012.2214050
[22] A. M. Adeshina, S. F. A. Razak, S. Yogarayan, and S. Sayeed, "MEASURING FIDELITY OF STEGANOGRAPHY APPROACH IN SECURING CLINICAL DATA SHARING PLATFORM USING PEAK SIGNAL TO NOISE RATIO (PSNR) AND STRUCTURAL SIMILARITY INDEX MEASURE (SSIM)," *Informatica*, vol. 49, no. 11, Jan. 2025. doi: https://doi.org/10.31449/inf.v49i11.5661
[23] M. A. VandeHaar, "CHALLENGES AND OPPORTUNITIES IN CYTOPATHOLOGY ARTIFICIAL INTELLIGENCE," *Bioengineering*, vol. 12, no. 2, p. 176, Feb. 2025.
[24] N. Youneszade, M. Marjani, and C. P. Pei, "DEEP LEARNING IN CERVICAL CANCER DIAGNOSIS: ARCHITECTURE, OPPORTUNITIES, AND OPEN RESEARCH CHALLENGES," *IEEE Access*, vol. 11, pp. 6133–6149, 2023. doi: https://doi.org/10.1109/access.2023.3235833
[25] K. P. Win, Y. Kitjaidure, K. Hamamoto, and T. Myo Aung, "COMPUTER-ASSISTED SCREENING FOR CERVICAL CANCER USING DIGITAL IMAGE PROCESSING OF PAP SMEAR IMAGES," *Applied Sciences*, vol. 10, no. 5, p. 1800, Mar. 2020. doi: https://doi.org/10.3390/app10051800
[26] E. Hussain, L. B. H. B. Mahanta, and C. Ray Das, "LIQUID BASED CYTOLOGY PAP SMEAR IMAGES FOR MULTI-CLASS DIAGNOSIS OF CERVICAL CANCER," *Mendeley Data, V2*, 2019. doi: https://doi.org/10.1016/j.dib.2020.105589
[27] O. Attallah, "CERCAN·NET: CERVICAL CANCER CLASSIFICATION MODEL VIA MULTI-LAYER FEATURE ENSEMBLES OF LIGHTWEIGHT CNNS AND TRANSFER LEARNING," *Expert Syst Appl*, vol. 229, p. 120624, Nov. 2023. doi: https://doi.org/10.1016/j.eswa.2023.120624
[28] T. Wu, E. Lucas, F. Zhao, P. Basu, and Y. Qiao, "ARTIFICIAL INTELLIGENCE STRENGTHENES CERVICAL CANCER SCREENING – PRESENT AND FUTURE," *Cancer Biol Med*, pp. 1–16, Sep. 2024. doi: https://doi.org/10.20892/j.issn.2095-3941.2024.0198
[29] N. Van Thieu and S. Mirjalili, "MEALPY: AN OPEN-SOURCE LIBRARY FOR LATEST META-HEURISTIC ALGORITHMS IN PYTHON," *Journal of Systems Architecture*, vol. 139, p. 102871, Jun. 2023. doi: https://doi.org/10.1016/j.sysarc.2023.102871
[30] B. Goyal, A. Dogra, S. Agrawal, B. S. Sohi, and A. Sharma, "IMAGE DENOISING REVIEW: FROM CLASSICAL TO STATE-OF-THE-ART APPROACHES," *Information Fusion*, vol. 55, pp. 220–244, Mar. 2020. doi: https://doi.org/10.1016/j.inffus.2019.09.003
[31] B. Maiseli, "NONLINEAR ANISOTROPIC DIFFUSION METHODS FOR IMAGE DENOISING PROBLEMS: CHALLENGES AND FUTURE RESEARCH OPPORTUNITIES," *Array*, vol. 17, p. 100265, Mar. 2023. doi: https://doi.org/10.1016/j.array.2022.100265
[32] V. Malathi and A. Manikandan, "AN UNDERWATER IMAGE ENHANCEMENT BY REDUCING SPECKLE NOISE USING MODIFIED ANISOTROPIC DIFFUSION FILTER," *International Journal of Electrical and Computer Engineering (IJECE)*, vol. 13, no. 6, p. 6361, Dec. 2023. doi: https://doi.org/10.11591/ijece.v13i6.pp6361-6368
[33] N. Mehta, S. V. A. V. Prasad, and L. Arya, "NOISE REDUCING PERFORMANCE OF ANISOTROPIC DIFFUSION FILTER AND CIRCULAR MEDIAN FILTER IN DIGITAL IMAGES," *International Journal of Digital Signals and Smart Systems*, vol. 4, no. 1/2/3, p. 171, 2020. doi: https://doi.org/10.1504/ijdsss.2020.106081
[34] J. Tang, G. Liu, and Q. Pan, "A REVIEW ON REPRESENTATIVE SWARM INTELLIGENCE ALGORITHMS FOR SOLVING OPTIMIZATION PROBLEMS: APPLICATIONS AND TRENDS," *IEEE/CAA Journal of Automatica Sinica*, vol. 8, no. 10, pp. 1627–1643, Oct. 2021. doi: https://doi.org/10.1109/jas.2021.1004129
[35] M. Sharma and P. Kaur, "A COMPREHENSIVE ANALYSIS OF NATURE-INSPIRED META-HEURISTIC TECHNIQUES FOR FEATURE SELECTION PROBLEM," *Archives of Computational Methods in Engineering*, vol. 28, no. 3, pp. 1103–1127, May 2021. doi: https://doi.org/10.1007/s11831-020-09412-6
[36] A. Agrawal, D. Garg, R. Sethi, and A. K. Shrivastava, "OPTIMUM REDUNDANCY ALLOCATION USING SPIDER MONKEY OPTIMIZATION," *Soft comput*, vol. 27, no. 21, pp. 15595–15608, Nov. 2023. doi: https://doi.org/10.1007/s00500-023-08746-0
[37] J. C. Bansal, H. Sharma, S. S. Jadon, and M. Clerc, "SPIDER MONKEY OPTIMIZATION ALGORITHM FOR NUMERICAL OPTIMIZATION," *Memet Comput*, vol. 6, no. 1, pp. 31–47, Mar. 2014. doi: https://doi.org/10.1007/s12293-013-0128-0
[38] U. Sara, M. Akter, and M. S. Uddin, "IMAGE QUALITY ASSESSMENT THROUGH FSIM, SSIM, MSE AND PSNR - A COMPARATIVE STUDY," *Journal of Computer and Communications*, vol. 07, no. 03, pp. 8–18, 2019. doi: https://doi.org/10.4236/jcc.2019.73002

[39] H. M. Qassim, N. M. Basheer, and M. N. Farhan, "BRIGHTNESS PRESERVING ENHANCEMENT FOR DENTAL DIGITAL X-RAY IMAGES BASED ON ENTROPY AND HISTOGRAM ANALYSIS," *Journal of Applied Science and Engineering*, vol. 22, no. 1, pp. 187–194, 2019.

[40] L. S. Chow and H. Rajagopal, "MODIFIED-BRISQUE AS NO REFERENCE IMAGE QUALITY ASSESSMENT FOR STRUCTURAL MR IMAGES," *Magn Reson Imaging*, vol. 43, pp. 74–87, Nov. 2017. doi: https://doi.org/10.1016/j.mri.2017.07.016